Dipole-excited surface plasmons in metallic nanoparticles: Engineering decay dynamics within the discrete-dipole approximation

Stefania D'Agostino,[1] Fabio Della Sala,[2,3] and Lucio Claudio Andreani[1]
[1]*Dipartimento di Fisica, Università di Pavia, via Bassi 6, I-27100 Pavia, Italy*
[2]*National Nanotechnology Laboratory (NNL), Istituto Nanoscienze-CNR, Via per Arnesano 16, I-73100 Lecce, Italy*
[3]*Center for Biomolecular Nanotechnologies @UNILE, Istituto Italiano di Tecnologia, Via Barsanti, I-73010 Arnesano, Italy*
(Received 9 September 2012; revised manuscript received 26 February 2013; published 8 May 2013)

A theoretical control of the electromagnetic coupling between localized surface plasmons and pointlike sources of radiation is a relevant topic in nanoscience and nanophotonics. In this paper a numerical approach based on the discrete dipole approximation is presented as a practical and reliable computational tool to study the decay dynamics of a dipole when it is located in the near proximities of metallic nanoparticles whose shapes do not allow a fully analytical treatment. The method is first applied to Ag nanospheres and nanoshells, which represent two analytically solvable cases, and it is shown to lead to a very good agreement with exact results. The approach is then used to consider the response, in terms of perturbations induced on the radiative and nonradiative decay rates, of elongated nanoparticles, like Ag prolate spheroids and nanocones. Results demonstrate how the optical response of conically shaped nanoparticles can be affected by the distance and the orientation of the emitter of radiation, as well as by other geometrical parameters. The particular symmetry of these plasmonic objects results in peculiar features: the absorption efficiencies of the modes depend on the distance of the source of radiation in a counterintuitive way, and this is explained in terms of the excited charge density distributions. The possibility to simulate arbitrary-shaped nanostructures and several dipole-metal configurations presented here, could thus open new avenues for an aware use of surface plasmons in fluorescence spectroscopy applications or single photon emission studies.

DOI: 10.1103/PhysRevB.87.205413 PACS number(s): 73.20.Mf, 78.66.Bz, 78.67.−n

I. INTRODUCTION

Fluorescence processes involving the emission of light by fluorophores or colloidal quantum dots (QDs) can be influenced by changes either in the excitation rate or in the quantum yield of the emitter. Over the last years there has been a considerable effort to control the modification of spontaneous emission, and the radiative decay rate engineering (RDE) has become a central issue in nanophotonics. The development of nano-optics techniques has affirmed the importance of exploiting plasmonic nanoantennas, like metallic nanoparticles or nanotips, to modify the excited-state lifetime,[1] the fluorescence intensity,[1–9] and the radiation distribution[7,10] of isolated emitters. Thanks to the highly confined electromagnetic resonances following from the response of free electrons,[2] metallic nanoparticles or nanostructures are able to strongly perturb the electromagnetic fields in their surroundings and to modify both the excitation and the emission rates of proximate fluorophores, chromophores, and QDs.[11] Abundant experimental evidence shows that the internal dynamics of an emitting system can be controlled in a photonic environment that is resonant with radiative transitions of the source, and effects such as surface-enhanced Raman scattering or surface-enhanced second harmonic generation are examples of this general phenomenon.[1,12–14] Moreover, due to their capabilities to strongly perturb the decay dynamics of an emitter, plasmonic components are promising candidates to enhance the capabilities of single photon sources.[15,16] Anyway, despite this, the problem of the electromagnetic coupling between a plasmonic object and a source of radiation located in its proximity still raises many open questions in molecular plasmonics, especially for complex nanoparticle shapes that do not lend themselves to an analytical treatment.

From a theoretical point of view, the investigation of electrodynamic coupling between molecules and metal nanoparticles can be treated with different levels of approximations according to the description used for the counterparts, and different options can be found in the literature. According to a widely used approach, the molecule is considered as a classical oscillating point dipole, and the metal nanoparticle as a continuous body described by its own frequency-dependent dielectric function.[3]

In an authoritative reference on the subject,[17] the use of classical electrodynamics and the approximation of the molecule with a dipole allow us to assess the lifetime of the molecular excited states in terms of the metal dielectric properties, the molecule-metal distance, and the molecule orientation with respect to a metal specimen considered as a semi-infinite metal bounded with a planar surface. This model, for distances of tens of nanometers from the surface, gives results in good agreement with the available experiments[18,19] and more generally it represents the most common way to describe the metal-molecule electrodynamic coupling problem in the literature.[20–24]

In regimes of short metal-molecule distances, other interactions become important, and chemical effects, such as orbital mixing or charge transfer between the excited molecule and the plasmonic system, or vice versa, must also be included in the treatment.[25–27] These interactions are sometimes mandatory for a complete understanding of some molecular plasmonics phenomena so that a more sophisticated method has been developed to study the coupling. It consists of exploiting the continuous body description of the metal and in treating the molecule atomistically by standard electronic structure methods, such as time dependent Hartree Fock (TDHF) or time

dependent density functional theory (TD-DFT), which include the electromagnetic interaction in the molecular Hamiltonian. At present, this approach has been explored mostly in the polarizable continuum model (PCM).[28,29]

Quantum electrodynamics description is surely the most appropriate theory to describe molecular plasmonics. Anyway, it brings into play quantities which can result not as intuitive as the classical ones. On the other side, classical electrodynamics turns out to be able to explain most of the observed phenomenology (also intrinsically quantum-mechanical processes).

In this work a classical electrodynamics description of a metal-emitter system is adopted to quantitatively study the perturbations induced by nanoparticles to the spontaneous decay rate of a single emitter assumed pointlike in a regime of weak coupling in which a macroscopic description of metal is assumed to be valid.[30] A discrete dipole approximation (DDA) based approach is presented as a useful and accurate tool to investigate coupling problems involving geometries not analytically solvable for which more accurate approaches (semi or fully *ab initio*) could result as prohibitive. The idea underlying the analysis consists of accurately describing the nanoparticle shape to get a faithful description of the optical response of the metallic component on the emitter, this being compulsory to quantify the perturbations induced on the decay dynamics of the dipole.

For a slab structure, for which the Green function is known analytically in Fourier space via angular spectrum decomposition[21,22,31] or for exciting fields that do not vary appreciably on the scale of a spherical particle,[21] similar approaches, based on the dyadic Green function calculation, have already been used in literature.[24,32–36] Other related studies to be mentioned are the CDM (coupled dipole method) analysis performed by Rahmani *et al.* on the effects of various structures deposited on a substrate,[37] the FEM (finite-element method) systematic investigation of Zhang *et al.* on infinite conical metal tips,[23] the multiple multipole (MMP) work of Liaw *et al.* on an electric dipole radiation in the presence of a nanoshell dimer,[38] the FDTD (finite difference time domain) studies of Ferrie *et al.* on gold-silica nanoparticles grafted with dye molecules,[39] the BEM (boundary element method) study of the coupling between a single emitter and a gold optical antenna of toroidal shape conduced by Teperik *et al.*,[40] the BEM-based MATLAB tool for the calculation of the decay rates for arbitrary-shaped nanoparticles developed by Hohenester and Trugler,[41] and finally those of Carminati *et al.*[20–22,24] and of Agio *et al.*[42–44]

Despite the vast literature in the field, to the author's knowledge, a crucial issue remains in demonstrating the reliability of a general-purpose numerical approach in calculating the total, radiative, and nonradiative decay rates of a metal-emitter system. In this paper a preliminary check performed in two different cases for which an analytical solution exists (spheres and nanoshells) shows an excellent agreement between exact and numerical results for the decay rate modification, thus placing the method on firm ground.

The analysis reported here aims at shedding light on the important contributions that elongated nanoparticles could provide in enhancing the decay rates of a dipole source. In particular, the optical behavior of 20 nm high Ag nanocones is investigated and put in relation to that obtained for prolate spheroids of same heights and different aspect ratios. The dependence of the response of this objects on the excitation conditions is then discussed in detail: the capability of an Ag nanocone to modify the lifetime of an emitter results in being strongly related to the dipole distance and orientation with respect to the tip, and only weakly affected by the presence of a second nanoparticle. Numerical results, obtained by studying the geometrical parameters, assess that the lifetime of a dipole as well as its fluorescence quantum yield can be significantly tailored by using the geometrical degrees of freedom of the system[45] and this could result in interest for time-resolved fluorescence spectroscopy[46,47] and scanning near-optical microscopy[48–53] applications.

The rest of this paper is organized as follows. In Sec. II we briefly outline the theoretical and computational method. In Sec. III we first compare the numerically computed decay rates for Ag nanospheres and nanoshells with the exact electrodynamical results that are known for these geometries. We then calculate dipole decay rate modifications in the presence of Ag prolate spheroids and compare them with those obtained with the improved Gersten and Nitzan (GN) model.[54–56] Finally, in Sec. IV we study in detail Ag nanocones by performing an analysis on the effects of dipole distance and orientation, the tip curvature radius, and the presence of a second reversed cone. The resonances appearing in the spectra are explained by recurring to the induced charge distributions. Section IV contains concluding remarks.

II. METHOD

A. Theory and implementation within the DDA framework

The entire work has been done in the framework of the discrete dipole approximation.[57] DDA is a numerical method which describes the metal as an array of polarizable dipolar elements organized on a cubic lattice (grid dipoles). The polarization of each element is the result of the interaction with the local electromagnetic field produced by all other elements plus the external field. Like the boundary element method, this method yields solutions of the electromagnetic field in response to an incident electric field in the frequency domain. A vast literature on numerical studies performed in the DDA framework exists, anyway it concerns the solution of the Maxwell problem for metallic structures excited with plane waves or radiations coming from infinitely far sources. Extending DDA to calculate dipole decay rates is the focus of this work.

In molecular plasmonics generally we have to deal with strongly variable electromagnetic fields emitted by molecules near metals. Since emitting molecules can be considered as pointlike radiating dipoles (their dimensions are in fact much smaller than electromagnetic wavelengths in the VIS-NIR range), then here we make an extension of the method to include dipolar fields as incident radiations. More in detail, we introduce into the parallel implementation *ADDA*,[58] the possibility to input the distribution of punctual sources (positions and components of the complex vectors describing the oscillating dipoles) and to generate the dipolar fields to apply, jointly or not to other external radiations, as excitation

of the target. After modifying in such a way the DDA code to include the effect of a punctual source, we then take care of the particle response and of the perturbations induced by it on the local field in the location of the emitting dipole.

If we assume a pointlike dipole $\tilde{\mathbf{p}}_0$ (here and hereafter complex quantities are indicated with a tilde) located at $\mathbf{r}_0$ and oscillating with frequency ω emitting electromagnetic radiation near a metallic nanoparticle, this nanoparticle will reflect and/or scatter back the radiation by generating an electric field $\tilde{\mathbf{E}}_{\text{scat}}$ given by $\tilde{\mathbf{E}}_{\text{scat}}(\mathbf{r}) = \tilde{\mathbf{G}}(\mathbf{r},\mathbf{r}_0,\omega)\cdot\tilde{\mathbf{p}}_0$, where $\tilde{\mathbf{G}}(\mathbf{r},\mathbf{r}_0,\omega)$ is the dyadic Green function or propagator which describes the electromagnetic response of the whole environment in point $\mathbf{r}$. Once the Green dyadic for a given system is known, all the relevant electromagnetic properties of the system can be derived.

In this work we make the assumption that the dipole does not change its strength with the interaction, anyway the code gives the option to consider the dipole as a dynamically polarizable point dependent on the local field $\tilde{\mathbf{p}}_0(\mathbf{r}_0) = \varepsilon_0\tilde{\alpha}\tilde{\mathbf{E}}(\mathbf{r}_0)$ so that the mutual interaction could be considered until the achievement of an electromagnetic balance between the counterparts.

The attention here is focused on the response field $\tilde{\mathbf{E}}_{\text{scat}}$ at $\mathbf{r}_0$. This can be described at several levels of approximation and in a few specific cases it can be found analytically.

In the work of Carminati *et al.*,[33] as an example, the nanoparticle itself is described in the dipole approximation and the Green function is calculated by

$$\tilde{\mathbf{G}}(\mathbf{r},\mathbf{r}_0,\omega) = \tilde{\mathbf{G}}_0(\mathbf{r},\mathbf{r}_0,\omega) + \tilde{\mathbf{G}}_0(\mathbf{r},\mathbf{r}_p,\omega)\cdot\tilde{\alpha}(\omega)\varepsilon_0\tilde{\mathbf{G}}_0(\mathbf{r}_p,\mathbf{r}_0,\omega), \quad (1)$$

where $\tilde{\alpha}(\omega)$ is the polarizability of the nanoparticle and $\mathbf{G}_0$ is the free-space Green function

$$\tilde{\mathbf{G}}_0(\mathbf{r},\mathbf{r}_0,\omega) = PV[k^2\mathbf{I}+\nabla\nabla]\frac{\exp(ikR)}{4\pi\varepsilon_0 R} - \frac{\mathbf{I}}{3\varepsilon_0}\delta(\mathbf{r}-\mathbf{r}_0), \quad (2)$$

where $\mathbf{I}$ is the unit dyadic and PV denotes the principal value.

Even if this approximation can represent a starting point for the solution of the dipole-metal interaction problem for small metallic objects, it has been shown to fail for large particles.[59] In a real situation, the model by Carminati *et al.* can be applied only for nanoparticle-molecule distances larger than a few (2–3) radii of the MNP, otherwise the total decay rates are largely underestimated. Higher multipole moment are needed for a correct description,[54,59] such as in the GN model.[54,60]

The idea underlying the present work is thus to better describe the local field in the dipole position by recurring to the numerical solution of the Maxwell problem obtainable within the DDA framework. By solving in a self-consistent way a system of $3N$ coupled complex equations, DDA gives the N polarizabilities $\tilde{\mathbf{p}}_i$ describing the polarization status of the target so that the scattered field experienced by the dipole[61] can be written as

$$\tilde{\mathbf{E}}_{\text{scat}}(\mathbf{r}_0) = \sum_{i=1}^{N}\tilde{\mathbf{G}}_0(\mathbf{r}_0,\mathbf{r}_i,\omega)\cdot\tilde{\mathbf{p}}_i. \quad (3)$$

In the weak-coupling regime, for which the spontaneous emission is irreversibly enhanced or reduced compared with its vacuum level,[62–65] the knowledge of this electric field allows us to compute the normalized spontaneous decay rate[32]

$$\frac{\Gamma}{\Gamma_0} = 1 + \frac{6\pi\varepsilon_0\tilde{\varepsilon}_B q_0}{k^3|\tilde{\mathbf{p}}_0|^2}\text{Im}[\tilde{\mathbf{p}}_0^*\cdot\tilde{\mathbf{E}}_{\text{scat}}(\mathbf{r}_0)], \quad (4)$$

where q_0 is the intrinsic quantum yield of the dipole, $\tilde{\varepsilon}_B$ is the relative dielectric constant of the background medium, and Γ_0 is the decay rate of a dipolar emitter with unitary quantum efficiency ($q_0 = 1$), corresponding to the total radiated power of a molecule in vacuum normalized to the energy

$$\Gamma_0 = \frac{P_0}{\hbar\omega} = \frac{1}{12\pi\varepsilon_0\tilde{\varepsilon}_B\hbar}|\tilde{\mathbf{p}}_0|^2 k^3. \quad (5)$$

Equation (4) expresses the modification of the lifetime of a molecule, known as the Purcell effect.[66] Purcell's prediction has been verified in different experimental settings such as close to plane interfaces,[67] in cavities[68] and photonic crystals,[69] and close to near-field optical probes.[70] It was realized that the modification of the lifetime is influenced by the radiative decay rate due to photon emission and by the nonradiative decay rate due to energy dissipation in the environment. For atoms or molecules close to metal surfaces both rates can be enhanced. Excited-state lifetimes of single molecules have been measured as a function of their separation from laser-irradiated metal boundaries and satisfactory agreement with theory has been achieved.[70,71]

If the photonic nanosystem is dissipative, the total decay rate Γ is the sum of radiative decay and the quenching rate induced by the lossy environment[5,6,12]

$$\frac{\Gamma}{\Gamma_0} = \frac{\Gamma_R}{\Gamma_0} + \frac{\Gamma_{\text{NR}}}{\Gamma_0}. \quad (6)$$

This relation can also be stated in terms of the optical reciprocity theorem,[60] i.e., of the relation between the ability of an antenna to emit electromagnetic waves and its ability to collect them. According to semiclassical theory,[54] the nonradiative decay rate derives from the (time-averaged) power absorbed by the nanoparticle P_{abs},

$$P_{\text{abs}} = \frac{\omega\varepsilon_0}{2}\text{Im}(\tilde{\varepsilon})\int_{V_p}|\tilde{\mathbf{E}}|^2\,dV. \quad (7)$$

By discretizing the nanoparticle within DDA, the normalized nonradiative decay rate Γ_{NR} becomes

$$\frac{\Gamma_{\text{NR}}}{\Gamma_0} = \frac{6\pi\varepsilon_0^2\tilde{\varepsilon}_B\text{Im}(\tilde{\varepsilon})}{|\tilde{\mathbf{p}}_0|^2 k^3}\left[\sum_{i=1}^{N}|\tilde{\mathbf{E}}_{\text{local}}(\mathbf{r}_i)|^2\cdot V_c\right], \quad (8)$$

where the summation is done on the N dipoles contributions and V_c is the volume of each cubic element.

The radiative decay rate can be finally obtained by computing the power radiated electromagnetically and dividing it by the photon energy $\hbar\omega$. According to classical radiation theory the power radiated by a system which is much smaller in size than the wavelength of the emitted light is determined by the electric dipole moment.[72] If the electric dipole moment of the

entire system (dipole of the NP plus external emitting dipole) is enhanced, so will the radiated power, the enhancement being proportional to the dipole amplification factor[54,60]

$$\frac{\Gamma_R}{\Gamma_0} = \frac{\varepsilon_0 \tilde{\varepsilon}_B}{|\tilde{\mathbf{p}}_0|^2} \left| \left[\sum_{i=1}^{N} \tilde{\mathbf{p}}_i (\mathbf{r}_i) \right] + \tilde{\mathbf{p}}_0 \right|^2 . \quad (9)$$

While (4) and (8) always give an exact expression of the total and nonradiative decay rates, in the limit of a fine discretization, the same is not true for the radiative contribution calculated with Eq. (9). Here the plasmonic structure jointly to the emitter acts as a unique radiating nanoantenna, but since the fields emitted by each dipole interfere with each other and with the fields directly emitted by the dipole, the phase difference between them should be considered for large objects or for big emitter-metal distances. Anyway here Eq. (9) gives values which correspond almost exactly (Fig. 3) to the differences between the total decay rate [Eq. (4)] and the nonradiative decay rate (8). In this approximation, once the radiative and the total decay rates are known, the quantum yield or quantum efficiency of the complete system can be calculated by the general formula

$$q = \frac{\Gamma_R/\Gamma_0}{(\Gamma_R + \Gamma_{NR} + \Gamma_{NR,0})/\Gamma_0} = \frac{\Gamma_R/\Gamma_0}{\Gamma/\Gamma_0 + (1 - q_0)}, \quad (10)$$

where $\Gamma_{NR,0}$ is due to the intrinsic losses mechanisms of the dipole.

B. Computational details and convergence

ADDA's main feature is the ability to run on a multiprocessor system by parallelizing a single DDA simulation. For each exciting frequency the scatterer is partitioned in slices parallel to the xy plane so that the run time is significantly reduced.[73] The routine of the dipolar field, used in this work, takes advantage of this parallelization: the incident field is calculated in the slices concurrently by the involved processors so that the impact on the whole simulation time can be considered negligible. Authors will make freely available this routine in the ADDA package so that the method could represent a valuable open-source tool for modeling in molecular plasmonics. For what concerns the choice of the interdipole distance or discretization parameter d_{int} (which in DDA represents the side of the elementary cube), the possibility to quickly ensure convergence depends on the size and the shape of the considered nanostructure. The results reported in the next sections are obtained by setting it to $d_{int} = 1/16$ nm.

For spherically shaped nanoparticles as well as for sharp objects (like the nanocone tip) special attention must be paid to the convergence problem. For spherically shaped nanoparticles, the adopted prescription for the discretization parameter $d_{int} = 1/16$ nm was proved to be good enough by recurring to the comparison with the analytical results (see Sec. III A). In Table I the normalized total, radiative, and nonradiative decay rates obtained for a 10 nm diameter Ag sphere excited by a dipole radially oriented (perpendicular) and oscillating at a 2 nm distance from the surface are reported as functions of d_{int}, for $\lambda_{exc} = 354$ nm. The reported values show that DDA results converge to the exact ones in the limit of a vanishing discretization and that the choice $d_{int} = 1/16$ nm yields results with an accuracy less than 5% for the normalized total and nonradiative decay rates. The error for the normalized radiative decay rate at $d_{int} = 1/16$ nm is higher (10%). However, we point out that, in this case, the normalized radiative decay rate is very small (three orders of magnitude smaller than the total decay rate). In other situations, e.g., when the dipole-surface distance is larger, the discretization error is reduced. For a dipole-surface distance of 5 nm, e.g., the error on the radiative decay rate at $d_{int} = 1/16$ nm, decreases to 6%. The numerical test in Table I is a very demanding one for a DDA simulation: in fact, while a smaller d_{int} increases the accuracy in the description of a spherical object with the DDA cartesian grid, the required computational effort is considerably increased. In Table II the DDA normalized decay rates obtained by improving the discretization level from $d_{int} = 1/8$ nm to $d = 1/32$ nm are reported for cones with $h = 20$ nm and aperture $\pi/13$ rad. As it can be observed, a good level of convergence can be achieved for a small metal-dipole distance and also for conically shaped nanoparticles. In fact, the deviation from $d_{int} = 1/16$ to $d_{int} = 1/32$ nm is about 1% for the normalized total and nonradiative decay rate. For the (very small) radiative one the accuracy is worse (as discussed above). Note again that this is the most extreme case considered in this work: in other simpler cases the accuracy will be better. This test thus validates the results given in Sec. IV.

TABLE I. Normalized total [Eq. (4)], radiative [Eq. (9)], and nonradiative [Eq. (8)] decay rates obtained for five different levels of discretization ($d_{int} = 1, 1/2, 1/4, 1/8$, and $1/16$ nm), for a 10 nm diameter Ag sphere, excited with a dipole oscillating perpendicularly with $\lambda_{exc} = 354$ nm at a distance of 2 nm from the surface. The exact electrodynamical theory values calculated for the same system are also reported as a reference.[55]

d_{int} (nm)	Γ/Γ_0	Γ_R/Γ_0	Γ_{NR}/Γ_0
1	17 877.6	4.3	17 866.5
1/2	9 982.8	7.3	9 974.5
1/4	10 984.7	10.8	10 973.7
1/8	12 987.8	13.3	12 946.7
1/16	14 044.8	14.9	14 029.9
Exact	14 757.1	16.6	14 740.4

TABLE II. Normalized total, radiative, and nonradiative decay rates obtained for three different levels of discretization ($d_{int} = 1/8$, $1/16$, and $1/32$ nm), for a 20 nm high Ag cone with aperture $\pi/13$ rad, excited with a dipole oscillating along the symmetry axis (perpendicular) with $\lambda_{exc} = 770$ nm at a distance of 2 nm from the tip.

d_{int} (nm)	Γ/Γ_0	Γ_R/Γ_0	Γ_{NR}/Γ_0
1/8	169 337.4	64.7	169 257.1
1/16	180 366.8	57.0	180 305.8
1/32	182 274.2	50.2	182 222.7

III. RESULTS: COMPARISON WITH OTHER MODELS

A. Ag nanospheres and nanoshells: Comparison with analytical results

As a starting point, the reliability of this DDA approach to compute the perturbations induced by a metallic nanoparticle on the dipole decay rates is tested for the benchmark case of a nanosphere. Simulations are done by considering a 10 nm diameter Ag sphere excited by a dipole oscillating either parallel or perpendicularly to the sphere (where for perpendicular orientation we intend the radial one). Results obtained for both orientations and $\lambda_{exc} = 354$ nm are reported in Fig. 1 and compared with those found with the exact electrodynamic theory (EET).[55]

As it can be noted in Fig. 1, the agreement between numerical and analytical decay rates (total, radiative, and nonradiative) as functions of dipole distance, turns out to be perfect for both orientations. The same check is done in Fig. 2 for an Ag nanoshell with a 10 nm diameter and a 2 nm wall thickness. In this case the curves are compared with those calculated by Moroz with the recursive transfer-matrix

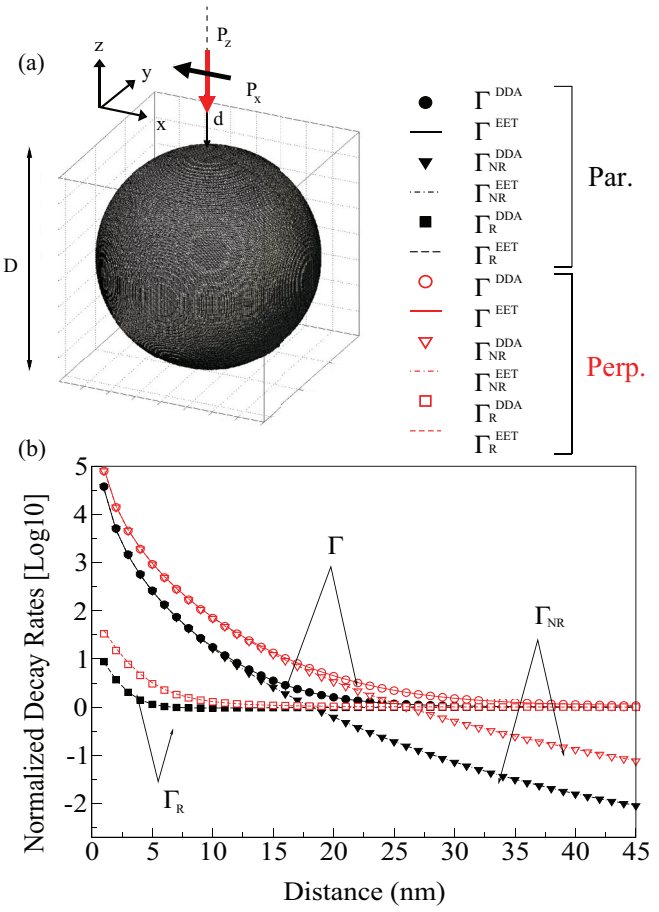

FIG. 1. (Color online) DDA and EET normalized decay rates for a 10 nm diameter Ag sphere excited by a dipole oriented parallel and perpendicularly to the surface [see schematization in (a)] and oscillating at $\lambda_{exc} = 354$ nm. (b) The numerical values are represented with symbols and analytical ones with lines. The interdipole distance used in the simulations is $d_{int} = 1/16$ nm and the values are reported in a decimal logarithmic scale.

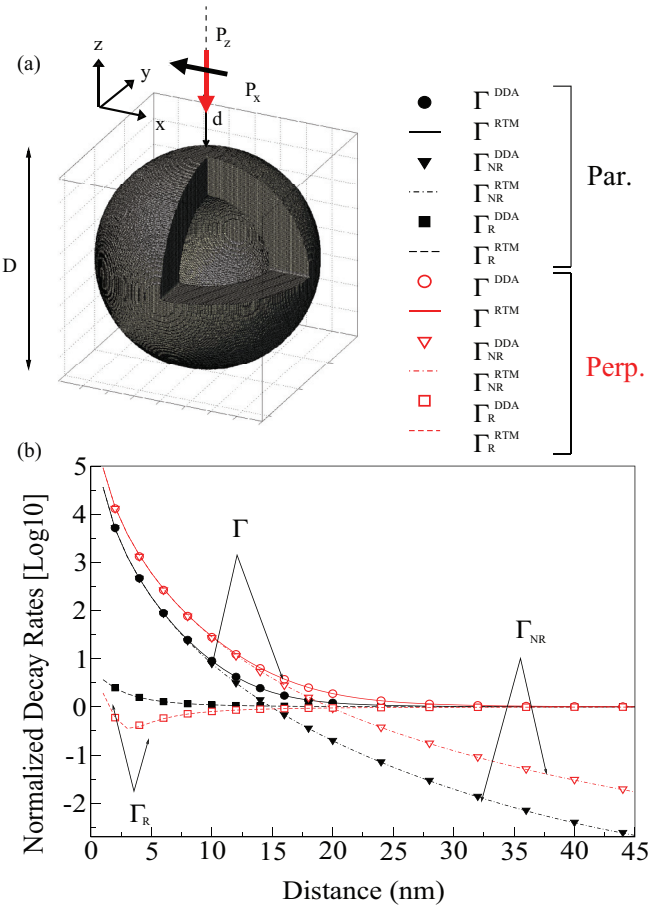

FIG. 2. (Color online) DDA and RTM normalized decay rates for a 10 nm diameter Ag shell with a wall thickness of 2 nm, excited by a dipole oriented parallel and perpendicularly to the surface [see schematization in (a)] and oscillating at $\lambda_{exc} = 354$ nm. (b) The numerical values are represented with symbols and analytical ones with lines. The interdipole distance used in the simulations is $d_{int} = 1/16$ nm and the values are reported in a decimal logarithmic scale.

solution (RTM) method[74] and the agreement is once again very satisfactory.

B. Ag prolate spheroids: Comparison with the improved Gersten and Nitzan model

While results on spheres and shells are elsewhere well analyzed,[55,74] the possibility to describe the metallic nanostructures numerically (through a fine discretization) allows us to apply the method to arbitrary-shaped nanoparticles and to solve cases that do not lend themselves easily to an analytical solution. For what concerns shapes solved only partially or with some approximations, we can mention oblate and prolate spheroids. The first analytical model on such kind of nanoparticles must be attributed to Gersten and Nitzan[54] who developed a quasistatic model in which retardation effects are treated as perturbations. This model was then improved by Mertens *et al.*[55,56] The improved GN model takes into account that the magnitude of the induced dipole moment is not only limited by absorption, but also by radiation losses.

Moreover, in this scheme the redshift of the dipole plasmon resonance caused by retardation of the depolarization field due to the finite dimensions of the sphere is implemented as well. Both these corrections to the original GN model are taken into account by an effective nanoparticle polarizability that differs from the electrostatic polarizability by a correction factor. To date it results in the best theoretical approach to treat the decay rate perturbations induced by spheroidal nanoparticles.

Specifically, the numerical analysis here is conduced on prolate Ag spheroids with a major axis of 20 nm and aspect ratios (a/b, with a and b, respectively, major and minor axes) 2 and 4, excited by perpendicular dipoles put at 2 nm from the particle surface. DDA results obtained for the normalized radiative and the total decay rate perturbations are reported, respectively, in Figs. 3(a) and 3(b) and compared with the improved GN model results,[55] where these are obtained by taking the optical data of Ag from Palik and by fixing the highest mode number of the expansion of the decay rate modification to $l = 60$. The agreement between the two methods is quite good. As it can be noted, differently from the case of an equivalent diameter sphere (not here reported), for prolate spheroids excited by a near dipole oscillating along the major axis, due to shape anisotropy we have the appearance of multiple resonances [Fig. 3(b)], the major one being a longitudinal dipole plasmon mode of the conduction electrons. This longitudinal dipole resonance becomes more and more distinguishable from the other ones at higher energies, at increasing aspect ratio of the spheroid, and it represents the unique mode contributing to the radiative decay rates for these small size prolate spheroids.

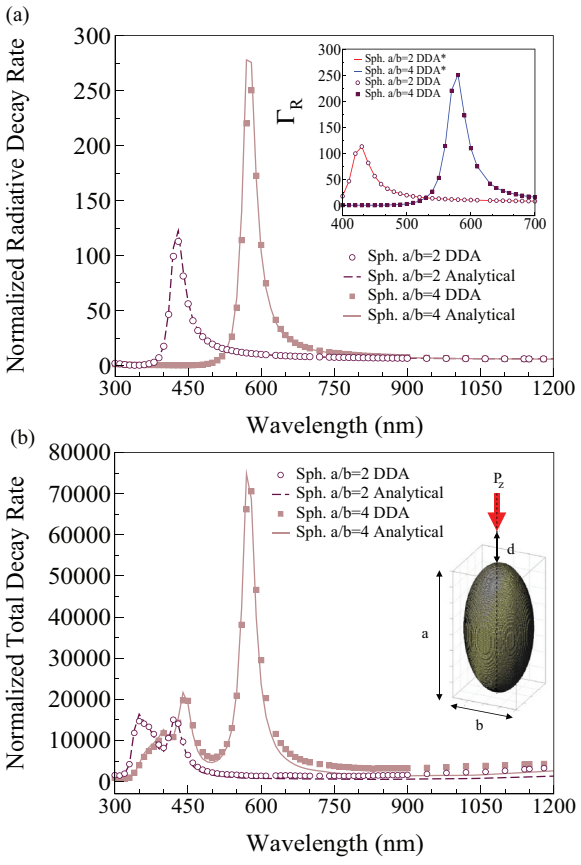

FIG. 3. (Color online) (a) Normalized radiative and (b) total decay rates obtained by DDA (symbols) and by the improved GN model (lines) for two prolate Ag spheroids with a major axis of 20 nm and two different aspect ratios a/b (2 and 4). Here a perpendicular dipole put at 2 nm from the surface is considered and an interdipole distance of 1/16 nm is used for the simulations. In the inset of (a) the Γ_R values calculated directly by Eq. (9) (DDA) are compared with the values obtained indirectly as the difference between the total and nonradiative decay rates $\left(\Gamma_R* = \Gamma - \Gamma_{\mathrm{NR}}, \mathrm{DDA}^*\right)$.

The DDA approach presented here allows us to go beyond the improved GN model in describing the multipole radiation by considering the metal polarization in a more faithful way. By comparing Γ_R calculated directly by Eq. (9) with the one obtained by difference between Γ and Γ_{NR} [inset in Fig. 3(a)], it can be observed how the approximation underlying Eq. (9) can be considered fully justified for small nanoparticles, like those here considered.

IV. RESULTS FOR Ag NANOCONES: A FULL NUMERICAL ENGINEERING

Until now we have just applied our method to well known cases. From here on we will focus on conically shaped nanoparticles, acting as nanoantennas: we will analyze 20 nm high Ag nanocones excited by a dipole oscillating at several distances from the tip (Sec. IV A), with different orientations with respect to the base plane (Sec. IV B), with various tip curvatures (Sec. IV C), or reversed with respect to the reference cone (Sec. IV D). In this work the considered radii of curvature of the Ag tips are very small ($r_c \simeq 0$ nm and $r_c = 3$ nm), being well known that the field enhancement around a metallic tip increases dramatically when r_c decreases.[23] Moreover, we know from literature that state-of-the-art fabrication techniques allow us to reach values of the radius of curvature of tapered waveguides below 5 nm.[75,76]

Analyzing the plasmonic modes in a frequency-domain framework is not a trivial point. For this reason, to clarify the nature of the resonances of these conically shaped nanostructures, in this section we will recur to the charge distribution inside the metal. To do this we have extended the DDA code in order to directly compute the charge distribution inside the metallic target by simply starting from the N DDA polarization densities $\tilde{P}_i$, defined as the grid dipoles $\tilde{\mathbf{p}}_i$ for cube volume V. In particular, we quantify the charge density at any point $\mathbf{r}_i$ by applying the relation

$$\tilde{\rho}_i\left(\mathbf{r}_i, \lambda_{\mathrm{exc}}\right) = -\nabla \cdot \tilde{\mathbf{P}}_{\mathbf{i}}\left(\mathbf{r}_i, \lambda_{\mathrm{exc}}\right). \tag{11}$$

This approach provides direct access to the real volume charge density inside the analyzed metallic nanostructure and can be very helpful for the identification of the multipolar plasmon modes inside complex plasmonic nanostructures.[77] Since the obtained quantity is defined up to an arbitrary phase factor [$\tilde{\rho}(\mathbf{r}_i) = \rho(\mathbf{r}_i)e^{i\theta}$], corresponding to $t \neq 0$ in the time dependence, for graphical reasons we choose the phase factor in order for $\tilde{\rho}$ to be real. To have an intuitive picture of the induced electronic charge, $\rho(\mathbf{r})$ is then transformed into a one-variable function $Q(x)$ by integrating it on slices with a thickness $d = 1$ nm perpendicular to the chosen

direction

$$Q(x,\lambda_{\rm exc}) = \int_{x-d/2}^{x+d/2} \iint \rho_i(x',y',z',\lambda_{\rm exc})dx'dy'dz'. \quad (12)$$

An alternative description to clarify the nature of the modes could be to employ the phase of the electromagnetic field and its nodes inside the nanoparticle.[78,79]

A. Effects of dipole distance

Similarly to what was observed for the prolate spheroids, we expect sharp nanocones to support a series of resonances associated with higher-order surface plasmon modes. In Fig. 4 the absorption efficiency spectra obtained for a fixed cone excited by a dipole at increasing distance from the tip (from 2 to 50 nm, along the symmetry axis) are reported and compared with the spectrum calculated by considering a plane wave impacting laterally (along the y direction) and polarized along the z direction. When the source of radiation is very close to the tip (2 nm), only the lower-energy (dipole) mode can be excited at a wavelength of 770 nm ($\lambda_1^{\perp}$). Otherwise, by moving away from the tip, the spectrum becomes broader with a shoulder on the short-wavelength side of the dipolar resonance until a second peak appears at 580 nm ($\lambda_2^{\perp}$). For larger distances ($d > 20$ nm), a third peak emerges at 490 nm ($\lambda_3^{\perp}$) and it becomes more and more evident on increasing d. For a 50 nm far emitter, the field induced by the dipole behaves like the one induced by a plane wave with the same polarization properties (z polarization).

This dependence of the spectrum on the emitter-metal separation seems to be counterintuitive and very interesting: an explanation can be found in the charge distributions reported in Figs. 4(b)–4(d). As it can be observed from the charge dislocation along the height of the cone, the resonance at 770 nm looks like a $l = 1$ mode with an important net dipole moment [Figs. 4(d)]: this can therefore be excited by both radiation sources considered here. The resonances appearing at higher energies (580 and 490 nm) instead, seem to be

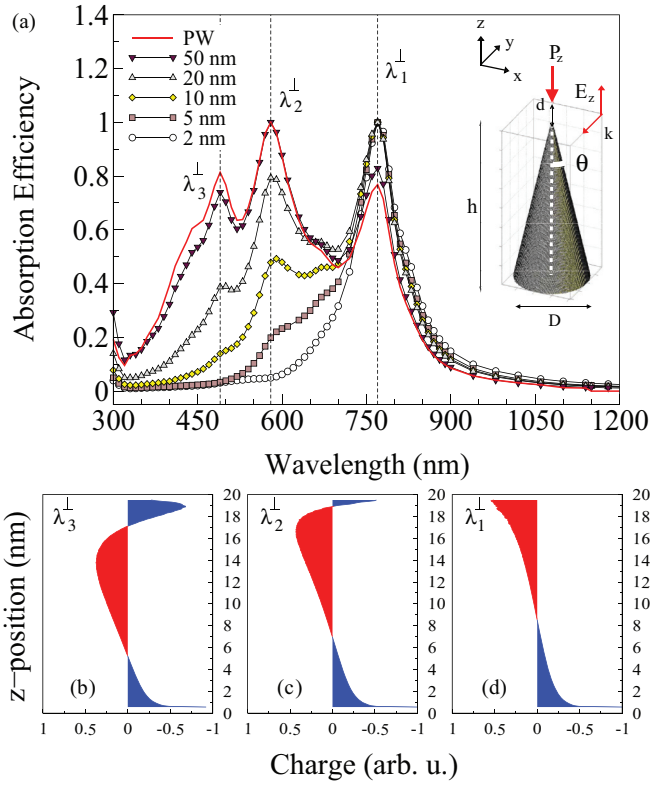

FIG. 4. (Color online) (a) Absorption efficiency spectra obtained by exciting an Ag nanocone with a perpendicular dipole oscillating at several distances (in nanometers) from the tip. The cone has height $h = 20$ nm, aperture $\theta = \pi/13$ rad, and a base $D = 2h\tan(\theta)$. The spectrum obtained by considering a plane wave propagating along y and polarized along the z direction is also reported for comparison (PW). For visualization purposes each spectrum is normalized to its maximum value. (b)–(d) Charge distributions along the symmetry direction of the cone for the three resonances in the PW spectrum in (a): $\lambda_1^{\perp} = 770$ nm (b), $\lambda_2^{\perp} = 580$ nm (c), and $\lambda_3^{\perp} = 490$ nm (d). The values are normalized to the maximum value registered for the three resonances.

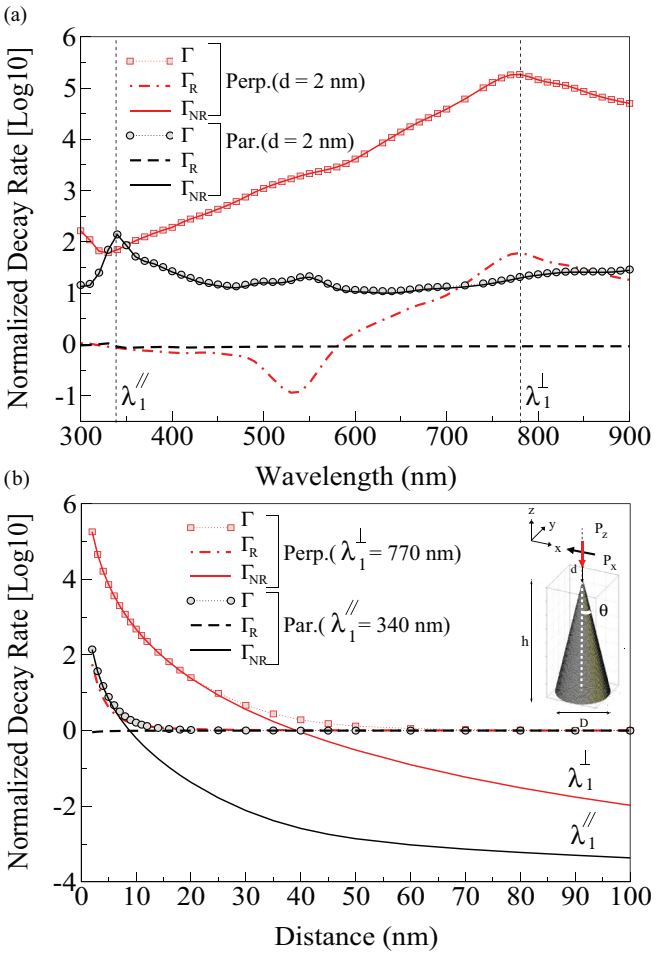

FIG. 5. (Color online) (a) Normalized decay rates as functions of the emitter wavelength for a cone with $h = 20$ nm and aperture $\theta = \pi/13$ rad excited with the dipole $\tilde{\mathbf{p}}$ oscillating in both configurations shown in the sketch in (b). (b) Total, radiative, and nonradiative decay rates as functions of the distance of the emitter from the tip of the cone for the two polarizations. The exciting wavelengths in (b) correspond to the peaks appearing in (a), $\lambda_1^{\parallel} = 340$ nm (parallel) and $\lambda_1^{\perp} = 770$ nm (perpendicular). All the decay rates are normalized to the free-space total decay rate of the dipole (Γ_0) and are reported in a decimal logarithmic scale.

related to higher order modes, being the number of nodes in the charge distribution larger that one [Figs. 4(b) and 4(c)]. In both these resonances the two asymmetrically distributed regions of induced charge radiate as antiparallel dipoles but, differently from what happens for structures symmetric along the radiation polarization, they do not yield a vanishing net dipole along z. The inversion asymmetry of the nanocone with respect to a xy plane can thus be considered responsible for the electromagnetic coupling of the modes with even l (dark in a symmetric structure) with a plane wave radiation.

When the nanocone is excited by a dipolar field, the excitation spectra have a marked dependence on distance. If from symmetry considerations the dipole could couple with all the resonances excited by the plane wave, the behavior of the field lines evolves with the distance between the dipole source and the tip, causing the appearance of resonances at increasing metal-dipole distance. In the next proximity of the dipole (2 nm) the dipolar field is almost completely directed along z, this pushes the electrons toward the tip and creates depletion areas along the edges of the base [see Fig. 7(a)]. For larger distances the field can also produce more complex distributions with electrons spilled up and down: a central depletion area localized near the tip can thus be generated. The results of Fig. 4 therefore show that a small conically shaped nanoparticle like the one here analyzed can support several plasmonic resonances in the VIS spectral range and that the higher-order resonances can be excited, provided the distance between the dipole and the tip is properly tailored. This can be very useful to get information on the metal-emitter distance in experimental setups: in a scanning microscopy configuration the distance between the tip and the sample could be determined from the spectral dependence of the measured decay rates or absorption efficiency.

B. Effects of dipole orientation

We now place the oscillating dipole at 2 nm from the same cone in Fig. 4 and consider two orientations for the exciting dipole with respect to the cone base. As it can be observed in Fig. 5(a), the two decay spectra obtained for the parallel and the perpendicular orientations are substantially different: for the former a small peak appears at 340 nm ($\lambda_1^{\parallel}$), while for the latter we can observe a strong resonance at 770 nm ($\lambda_1^{\perp}$). It must be noted that in Fig. 5(a), for visualization purpose, the spectra are reported in a decimal logarithmic scale and the maximum values go from 139 for the parallel case, to 180 367 for the perpendicular one. Thus the perpendicular orientation strongly dominates the decay rate variations, with changes of the order of 10^5. This important increase of the decay rate could strongly decrease the lifetime of many emitters currently available such as nitrogen-vacancy (NV) centers in diamond which have typical lifetimes of 10 ns. For practical applications, in fact an emission rate on the order of picoseconds or femptoseconds is desirable to take full advantage of the new generation of mode-locked lasers with high repetition rates.[15]

For applications to fluorescence spectroscopy measurements it is also interesting to study the decrease of the decay rates with the distance of the source from the metal. The normalized total (Γ), radiative (Γ_R), and nonradiative (Γ_{NR}) decay rates for the two orientations at the resonances ($\lambda_1^{\parallel} = 340$ nm and $\lambda_1^{\perp} = 770$ nm), are thus reported in Fig. 5(b), as logarithmic functions of the dipole distance d from the cone tip.

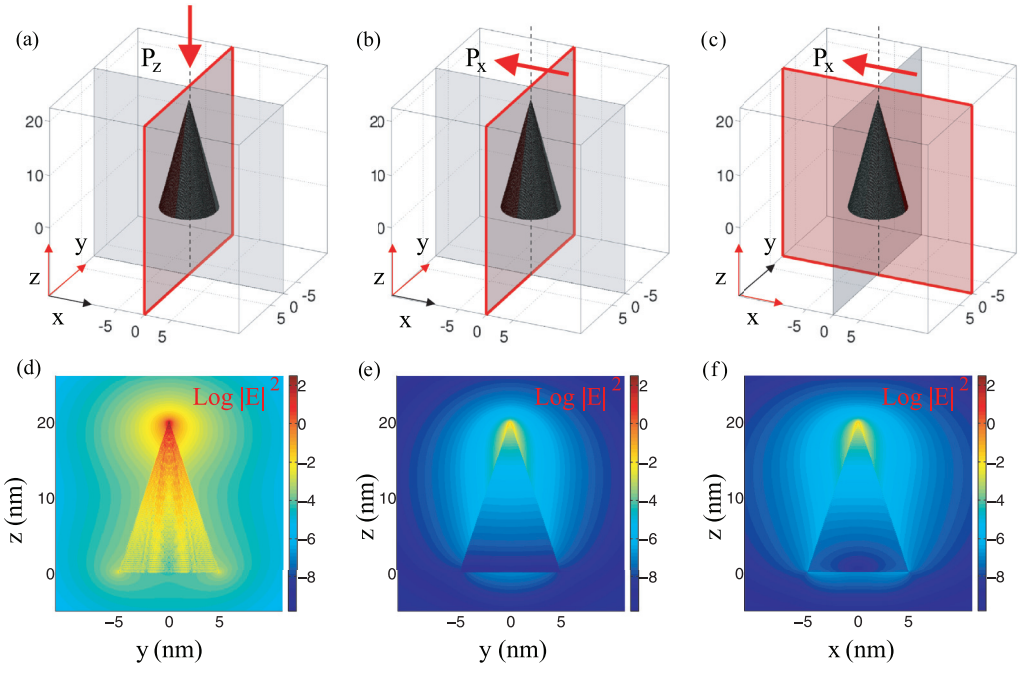

FIG. 6. (Color online) (a)–(c) The analyzed systems are schematized as references for the maps reported below (d)–(f), which display the squared moduli of the scattered field $|\tilde{\mathbf{E}}_{\text{scat}}|^2$, normalized to $|\tilde{\mathbf{p}}_0|^2$, and calculated inside and outside a cone with $h = 20$ nm and aperture $\theta = \pi/13$ rad excited by a dipole oscillating perpendicularly ($\lambda_1^{\perp} = 770$ nm) (d) and parallel ($\lambda_1^{\parallel} = 340$ nm) to the cone base (e) and (f) at a distance of 2 nm from the tip of the cone. The values are in a decimal logarithmic scale.

Besides the huge spread in the starting values (for the nearest distance $d = 2$ nm) for the perpendicular case, in Fig. 5(b) we observe a slower decrease of the decay rates at increasing distance (total and nonradiative are almost indistinguishable), compared to the parallel case in which we have curves which rapidly reach the limiting values for $d \to \infty$.

Data in Fig. 5 have a twofold validity: in time-resolved fluorescence measurements we could use sharp Ag tips to monitor either the distance or the orientation of pointlike sources by knowing just one of these variables. From the changes in the lifetime of molecules with a known free-space decay rate, as an example, it could result in possibly extracting reliable information on their distance from the metal, once the orientations are known (e.g., from *ab initio* quantum-mechanical simulations). Vice versa, once the distance is known, the orientation of the dipole can be found out. In general this kind of theoretical studies allow experimentalists to extract information by starting from a comparison between the detected signals and the simulated quantities: in a recent work on ultrabright bow-tie nanoaperture antenna probes, as an example, the 3D vectorial mapping of the near-field distribution is put in relation to the orientations of the molecules emitting fluorescence.[80]

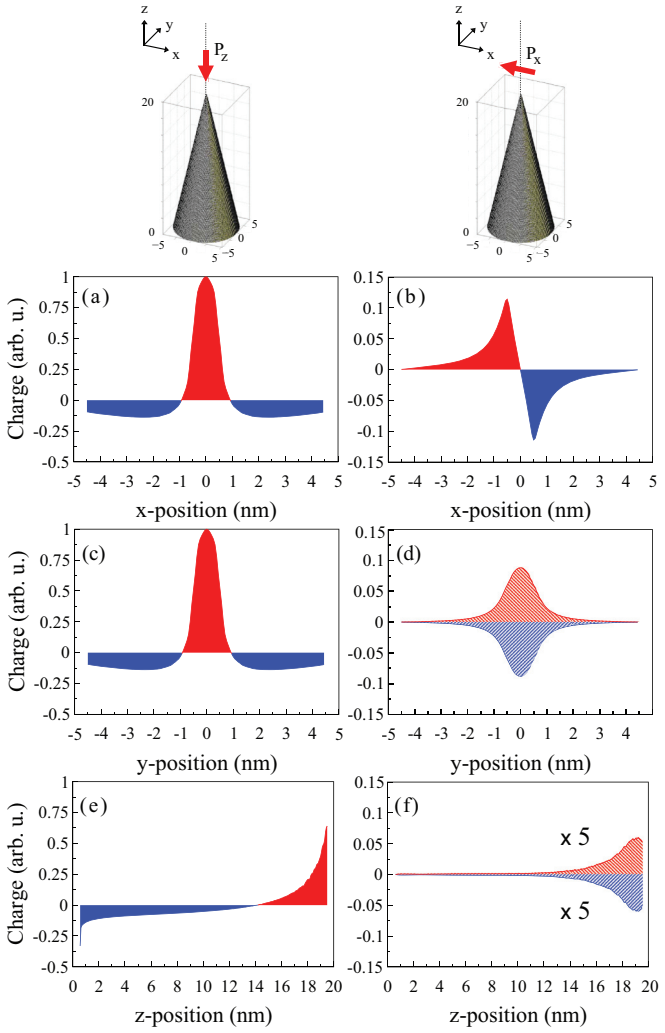

FIG. 7. (Color online) Charge accumulated in 1 nm thick layers cutting the cone along the three directions for the perpendicular [(a), (c), and (e)] and the parallel [(b), (d), and (f)] orientations of the emitter oscillating at $\lambda_1^{\perp} = 770$ nm and $\lambda_1^{\parallel} = 340$ nm, respectively. In panels (d) and (f) the charge is obtained by applying Eq. (12) but dividing the range of integral along the x position in two subsets ($x < 0$ and $x > 0$): since the charge density is odd along x, the two contributions cancel each other when calculated along the entire structure.

To get more detailed insight into the nature of the two kinds of resonance, we can look at the induced fields (Fig. 6) as well as at the charge distributions (Fig. 7). For what concerns the fields analysis, Fig. 6 shows the maps of the squared moduli of the scattered field along the yz and xz planes for both orientations in Fig. 5. From the color maps of the moduli in Fig. 6 we can get a clear idea of the important difference in the field enhancements which can be achieved in the two orientations: by moving from a perpendicular orientation (excited at $\lambda_1^{\perp} = 770$ nm) to a parallel one (excited at $\lambda_1^{\parallel} = 340$ nm) the scattered field not only decreases by 3 orders of magnitude but also changes its distribution in the space. In the first case [Fig. 6(a)] the field seems to be delocalized all over the structure, while in the second case [Figs. 6(b) and 6(c)] it appears localized in the upper region of the cone. Figure 7(b) explains the origin of such kind of field by presenting a clear dipolar distribution along the x direction, which corresponds to the emitter direction. Being odd along the x direction this charge distribution gives a null contribution if summed over the whole diameter of the base [see panels in Figs. 7(d) and 7(f)] and this null dipole momentum either along y or along z can justify the field profile in Figs. 6(b) and 6(c). The situation is completely different for the perpendicular case: the charge distribution now induced at 770 nm from a perpendicular dipole is even with respect to the symmetry axis. As already observed in Fig. 4(d) for a plane wave excitation, the resonance at 770 nm is due to a dipole along the symmetry axis of the cone [Fig. 7(e)]. We can thus observe that the orientation of the emitter, similar to that observed in other works,[20,80] is a crucial parameter to take into account.

In view of what was observed in Figs. 5, 6, and 7, we can affirm that with the same structure we can realize a sort of optical switching by simply tilting the dipole with respect to the symmetry axis: the same emitter at the same distance from the same tip can can change its radiative decay rate up to 2 orders by switching from the parallel to the perpendicular orientation.

C. Effects of the tip curvature

The dramatically different behavior between the perpendicular and parallel configurations is also confirmed by the different response that the two geometries show at increasing curvature radius of the tip, as illustrated in Fig. 8. The effect of changing the tip curvature can be understood as follows: for the case of perpendicular orientation, the exciting dipole probes the very tip of the cone, which is substantially modified by the effect of rounding. It is clear that rounding a tip or an edge must increase the resonance frequency of a surface plasmon, as the resonance frequency must tend to $\omega_p/\sqrt{2}$ from below. In the case of parallel orientation instead, the exciting field experiences the lateral surface of the cone, which is not

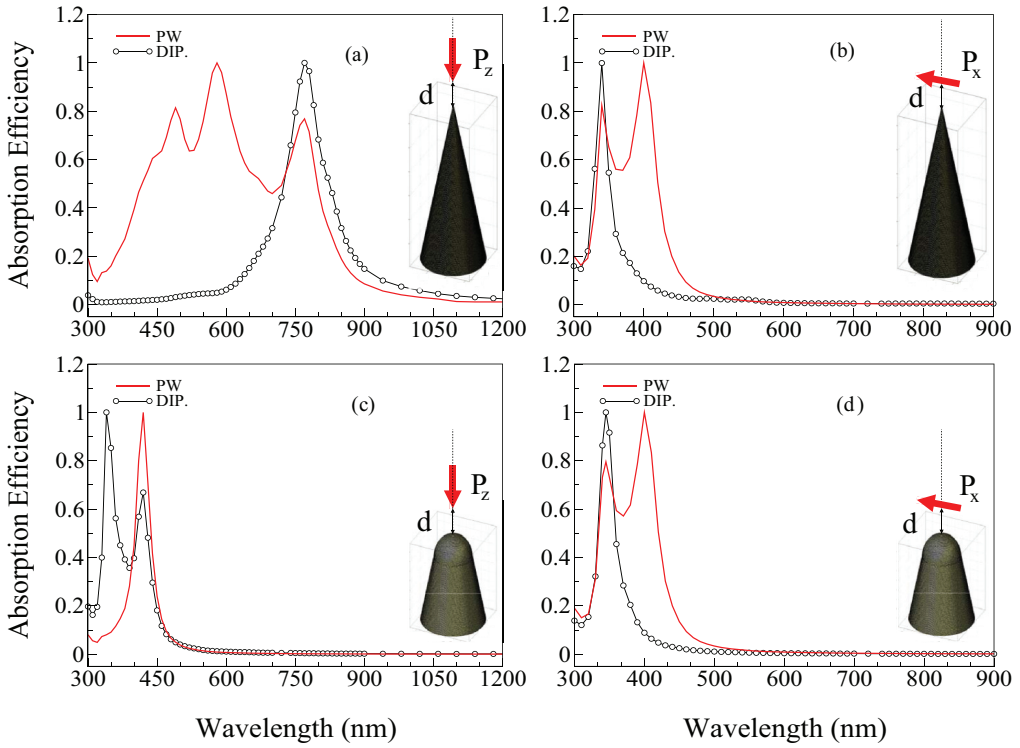

FIG. 8. (Color online) (a) Absorption efficiencies normalized to the maximum value for (a) a tip with $r_c \simeq 0$ nm excited by a perpendicular dipole, (b) a tip with $r_c \simeq 0$ nm excited by a parallel dipole, (c) a tip with $r_c = 3$ nm excited by a perpendicular dipole, and (d) a tip with $r_c = 3$ nm excited by a parallel dipole. Dipole is always put at 2 nm from the tip and in each panel the normalized absorption efficiency spectrum obtained for a plane wave excitation (PW) is also reported: in (a) and (c) the field propagates along y and oscillates along z, in (b) and (d) it propagates along z and oscillates along x.

modified by the tip rounding: this explains why the resonance frequencies in Figs. 8(b) and 8(d) remain the same.

Moreover, since the tip is specifically probed by a z polarized field, the response of the particle is strongly dependent on rounding in terms of number of excited modes (i.e., their selection rules) in addition to the mode frequencies. If we compare the plane wave spectra in Figs. 8(a) and 8(c) we can observe that more peaks are excited in the case of a sharp tip. This is because a cone with a sharp tip has a strong breaking of mirror symmetry with respect to the xy plane: thus, all modes are able to radiate and to couple to far-field excitation by a plane wave. This does not occur for the rounded cone, which is closer to a structure with mirror symmetry with respect to the xy plane: in such a structure, an even charge distribution has a vanishing net dipole along z, the corresponding mode being dark and not excited by a plane wave. This concept is well investigated in the work of Liu *et al.*,[79] where for a gold bipyramid the quadrupole mode disappears either in the Γ_R spectrum or in the plane wave cross section. This argument explains why less modes are excited by a plane wave for the rounded cone in Fig. 8(c). This selection rule does not apply for the dipole excitation, which breaks mirror symmetry by itself.[81]

D. Effects of mutual interaction in a double cone configuration

Finally, in this subsection we investigate the effect of a second reversed Ag cone coupled to the dipole-cone system until now under investigation. The cone is put at 4 nm from the bottom tip and a dipole aligned with the symmetry axis is supposed to oscillate in the middle of the gap. This double-cone configuration resembles the bow-tie nanoantenna with a sub-10 nm gap already produced by electron beam lithography.[82,83] Bow-tie dimer antennas are constituted of two triangles facing each other tip-to-tip.[84,85] They are being applied to enhance molecular fluorescence,[86] Raman scattering,[87,88] and for high-harmonic generation.[89]

Contrary to what is observed normally for dimers of nanoparticles in a near-field noncontact regime,[26,27,79] due to particular inversion symmetry of the system here, we cannot observe the appearance of hybrid modes corresponding to symmetric (bonding) and antisymmetric (antibonding) combinations of the individual modes at 770 nm ($\lambda_1^{\perp,S}$). As it can be observed in Fig. 9 we have only a peak at a larger wavelength ($\lambda_1^{\perp,D} = 785$ nm). Most probably this mode

TABLE III. Normalized total, radiative, and nonradiative decay rates obtained for the system in Fig. 9 for $\lambda_1^{\perp,D} = 785$ nm, $d_2 = 2$ nm, and five different d_1.

d_1 (nm)	Γ/Γ_0	Γ_R/Γ_0	Γ_{NR}/Γ_0
2	386 575.1	283.0	386 284.8
4	205 990.1	123.3	205 862.9
6	185 302.3	92.0	185 206.7
8	180 113.8	79.7	180 030.6
10	178 293.3	73.4	178 216.4
Single	176 633.0	59.0	176 570.4

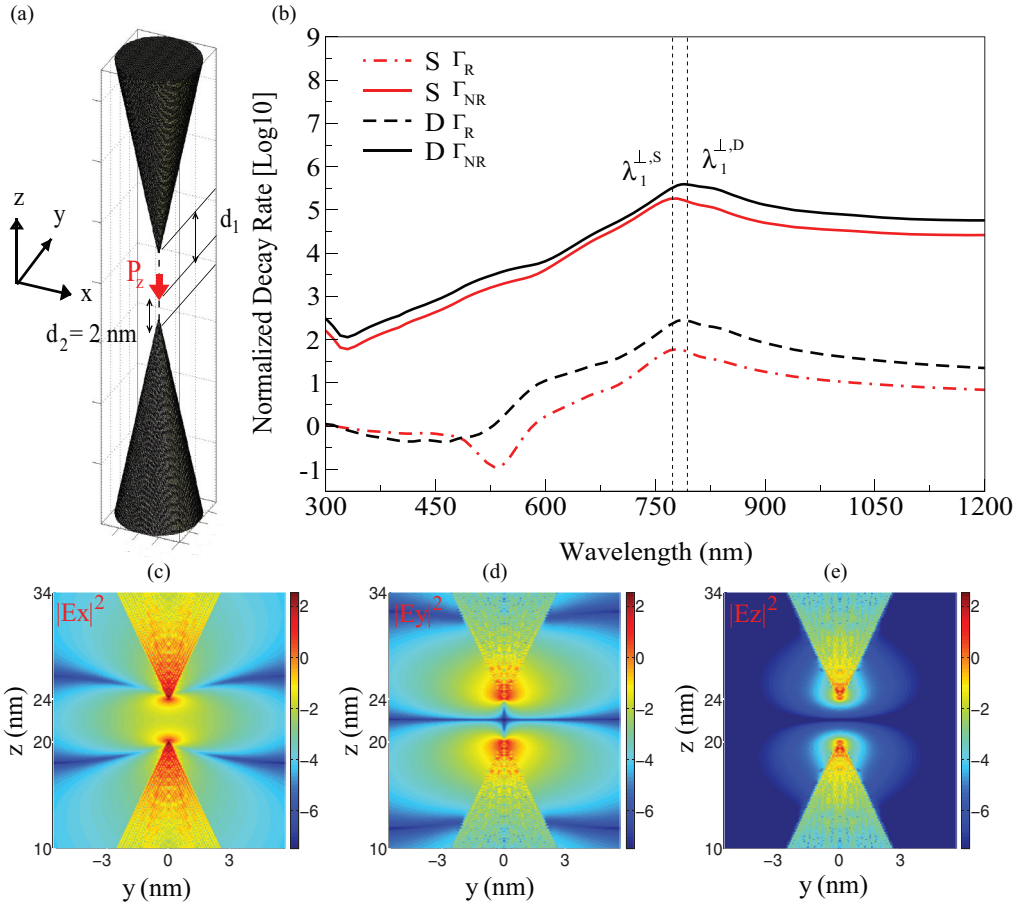

FIG. 9. (Color online) (a) Scheme of a double-cone configuration for a cone with $h = 20$ nm, aperture $\theta = \pi/13$ rad, and $r_c \simeq 0$ nm. (b) Radiative and nonradiative decay rates for a single cone (S) and a double one (D) with a 4 nm gap between the tips. In both the cases the emitter is located at 2 nm from the tip and oscillates along the symmetry axis. Maps in (c), (d), and (e) show $|E_{\mathrm{scat},x}|^2$, $|E_{\mathrm{scat},y}|^2$, and $|E_{\mathrm{scat},z}|^2$, respectively, in the plane yz for $\lambda_1^{\perp,D} = 785$ nm.

corresponds to the bonding mode in which both the dipoles are aligned along the symmetry axis and have the same direction. The maps of the three components of the scattered field in Fig. 9 can validate this statement.

The decay rate perturbations, calculated by fixing the distance of the dipole from the bottom tip at $d_2 = 2$ nm and varying the mutual distance between the dipole and the top cone d_1 are reported in Table III for $\lambda_1^{\perp,D} = 785$ nm. The decay rate changes cannot be interpreted in terms of a superposition of the electromagnetic fields generated by the isolated metallic structures: the presence of a second cone induces in fact some changes in the polarization of the previous one and thus a small enlargement of the E_z component of the field scattered back from the antenna to the emitter position. Anyway this turns out to be a short-range effect which rapidly vanishes when d_1 becomes a few nanometers larger than d_2.

V. CONCLUSIONS

The outcome of the analysis reported here is to validate a useful numerical approach, based on the discrete dipole approximation, to calculate the radiative and the nonradiative dynamics of a dipole emitter put in proximity of a metal nanoparticle. The results demonstrate that it is possible to achieve a good control of the lifetime and of the fluorescence quantum yield for a single dipole emitter, by simply tuning the spectral and the spatial degrees of freedom of the dipole-metal system. The method is general purpose and it represents a very satisfactory numerical approximation for small nanoparticles. In the limits of a fine discretization it allows us to reproduce the decay rate perturbations for analytically solved cases, e.g., spheres and nanoshells, to go beyond the improved GN model for prolate and oblate spheroids, and to solve the problem of the emitter-metal coupling for complex systems which have already been realized experimentally. It could also be combined with quantum electrodynamic treatments of the strong coupling regime,[90,91] again for complex shapes that cannot be treated analytically. With the fine discretization used in the present work, the numerical error is estimated to be of the order of a percent.

Here the computational approach is applied to study the optical response of 20 nm high Ag nanocones with a small aperture and a sharp tip to a dipole excitation, and in particular the dependence of the decay rates on the dipole position and orientation. The obtained results show the importance of this kind of plasmonics object in obtaining huge enhancements of the decay rates: if properly excited, in fact, a metallic nanocone is a suitable system to achieve significant modifications of

the spontaneous emission dynamics of a dipole. Favorable conditions are suggested by DDA simulations, which demonstrate the predominance of the perpendicular orientation for decay rate modifications and predict the distance dependence of the spectra. We believe these results to show the importance of a numerical engineering of decay rates exploiting surface plasmon resonances and in view of an aware experimental control of decay processes in time-resolved fluorescence spectroscopy.

ACKNOWLEDGMENTS

This work was funded by Fondazione Cariplo under Project No. 2010-0523 and by the European Research Council (ERC) Starting Grant Project DEDOM, Grant Agreement No. 207441. For computational facilities S.D. thanks Maxim Yurkin for the technical supported received on the code ADDA, the Italian Institute of Technology, and its cluster administrator Akhilesh Tanwar and finally the CINECA Consortium with its technical support (ISCRA Award No. HP10C1ZQTO, 2011).

[1] S. Kuhn, U. Hakanson, L. Rogobete, and V. Sandoghdar, Phys. Rev. Lett. **97**, 017402 (2006).
[2] J. A. Schuller, E. S. Barnard, W. S. Cai, Y. C. Yun, J. S. White, and M. L. Brongersma, Nat. Mater. **9**, 193 (2010).
[3] P. Anger, P. Bharadwaj, and L. Novotny, Phys. Rev. Lett. **96**, 113002 (2006).
[4] O. L. Muskens, V. Giannini, J. A. Sánchez-Gil, and J. Gómez Rivas, Nano Lett. **7**, 2871 (2007).
[5] H. Mertens, A. F. Koenderink, and A. Polman, Phys. Rev. B **76**, 115123 (2007).
[6] G. W. Ford and W. H. Weber, Phys. Rep. **113**, 195 (1984).
[7] T. H. Taminiau, F. D. Stefani, F. B. Segerink, and N. F. van Hulst, Nat. Photon. **2**, 234 (2008).
[8] A. Kinkhabwala, Z. Yu, S. Fan, Y. Avlavesich, K. Mullen, and W. E. Moerner, Nat. Photon. **3**, 654 (2009).
[9] D. E. Chang, A. S. Sorensen, E. A. Demler, and M. D. Lukin, Nat. Phys. **3**, 807 (2007).
[10] P. Muhlschlegel, H.-J. Eisler, O. J. F. Martin, B. Hecht, and D. W. Pohl, Science **308**, 1607 (2005).
[11] H. Metiu, Prog. Surf. Sci. **17**, 153 (1984).
[12] L. Novotny and B. Hecht, *Principles of Nano-Optics* (Cambridge University Press, New York, 2006).
[13] S. Kuhn, G. Mori, M. Agio, and V. Sandoghdar, Mol. Phys. **106**, 893 (2008).
[14] M. Moskovits, Rev. Mod. Phys. **57**, 783 (1985).
[15] R. Esteban, T. V. Teperik, and J. J. Greffet, Phys. Rev. Lett. **104**, 026802 (2010).
[16] M. E. Reimer, G. Bulgarini, N. Akopian, M. Hocevar, M. B. Bavinck, M. A. Verheijen, E. P. A. M. Bakkers, L. P. Kouwenhoven, and V. Zwiller, Nat. Commun. **3**, 737 (2012).
[17] R. R. Chance, A. Prock, and R. Silbey, Adv. Chem. Phys. **37**, 1 (1978).
[18] H. Kuhn, J. Chem. Phys. **53**, 101 (1970).
[19] K. H. Drexhage, in *Progress in Optics XII*, edited by E. Wolf (North-Holland, Amsterdam, 1974).
[20] M. Thomas, J.-J. Greffet, R. Carminati, and J. R. Arias-Gonzalez, Appl. Phys. Lett. **85**, 3863 (2004).
[21] C. Vandenbem, D. Brayer, L. S. Froufe-Perez, and R. Carminati, Phys. Rev. B **81**, 085444 (2010).
[22] C. Vandenbem, L. S. Froufe-Perez, and R. Carminati, J. Opt. A **11**, 114007 (2009).
[23] W. Zhang, X. Cuib, and O. J. F. Martin, J. Raman Spectrosc. **40**, 1338 (2009).
[24] L. S. Froufe-Perez, R. Carminati, and J. J. Saenz, Phys. Rev. A **76**, 013835 (2007).
[25] Y. Zhang, R. Zhang, Q. Wang, Z. Zhang, and Z. Haibo, Opt. Express **18**, 4316 (2010).
[26] K. J. Savage, M. M. Hawkeye, R. Esteban, A. G. Borisov, J. Aizpurua, and J. J. Baumberg, Nature (London) **491**, 574 (2012).
[27] R. Esteban, A. G. Borisov, P. Nordlander, and J. Aizpurua, Nat. Commun. **3**, 825 (2012).
[28] S. Miertuš, E. Scrocco, and J. Tomasi, Chem. Phys. **55**, 117 (1981).
[29] S. Corni and J. Tomasi, J. Chem. Phys. **117**, 7266 (2002).
[30] E. Castani, M. Boffety, and R. Carminati, Opt. Lett. **35**, 291 (2010).
[31] J. E. Sipe, J. Opt. Soc. Am. B **4**, 481 (1987).
[32] L. Novotny, Appl. Phys. Lett. **69**, 3806 (1996).
[33] R. Carminati, J.-J. Greffet, C. Henkel, and J. M. Vigoureux, Opt. Commun. **261**, 368 (2006).
[34] V. Giannini, J. A. Sanchez-Gil, O. L. Muskens, and J. Gomez Rivas, J. Opt. Soc. Am. B **26**, 1569 (2009).
[35] L. S. Froufe-Perez and R. Carminati, Phys. Rev. B **78**, 125403 (2008).
[36] L. S. Froufe-Prez and R. Carminati, Phys. Status Solidi A **205**, 1258 (2008).
[37] A. Rahmani, P. C. Chaumet, and F. de Fornel, Phys. Rev. A **63**, 023819 (2001).
[38] J.-W. Liaw, J.-H. Chen, C.-S. Chen, and M.-K. Kuo, Opt. Express **17**, 13532 (2009).
[39] M. Ferrie, N. Pinna, S. Ravaine, and R. A. Vallee, Opt. Express **19**, 17697 (2011).
[40] T. V. Teperik and A. Degiron, Phys. Rev. B **83**, 245408 (2011).
[41] U. Hohenester and A. Trügler, Comput. Phys. Commun. **183**, 370 (2012).
[42] L. Rogobete, F. Kaminski, M. Agio, and V. Sandoghdar, Opt. Lett. **32**, 1623 (2007).
[43] A. Mohammadi, V. Sandoghdar, and M. Agio, New J. Phys. **10**, 105015 (2008).
[44] A. Mohammadi, F. Kaminski, V. Sandoghdar, and M. Agio, J. Phys. Chem. C **114**, 7372 (2010).
[45] S. D'Agostino, F. Della Sala, and L. C. Andreani, Plasmonics (2013), doi: 10.1007/s11468-013-9512-3.
[46] R. R. Alfano, AIP Adv. **2**, 011103 (2012).
[47] M. R. Gartia, A. Hsiao, M. Sivaguru, Y. Chen, and G. L. Liu, Nanotechnology **22**, 365203 (2011).
[48] M. Specht, J. D. Pedarnig, W. M. Heckl, and T. W. Hansch, Phys. Rev. Lett. **68**, 476 (1992).
[49] F. Zenhausern, M. P. O'Boyle, and H. K. Wickramasinghe, Appl. Phys. Lett. **65**, 1623 (1994).
[50] R. Bachelot, P. Gleyzes, and A. C. Boccara, Appl. Opt. **36**, 2160 (1997).
[51] J. Boneberg, M. Ochmann, H.-J. Munzer, and P. Leiderer, Ultramicroscopy **71**, 345 (1998).

[52]L. Novotny, E. J. Sanchez, and X. S. Xie, Ultramicroscopy **71**, 21 (1998).
[53]M. Ashino and M. Ohtsu, Appl. Phys. Lett. **72**, 1299 (1998).
[54]J. Gersten and A. Nitzan, J. Chem. Phys. **75**, 1139 (1981).
[55]Code available at http://erbium.amolf.nl.
[56]H. Mertens and A. Polman, arXiv:0711.1591.
[57]B. T. Draine and P. J. Flatau, J. Opt. Soc. Am. A **11**, 1491 (1994).
[58]M. A. Yurkin and A. G. Hoekstra, *ADDA*, available at http://code.google.com/p/a-dda/.
[59]A. Moroz, Opt. Commun. **283**, 2277 (2010).
[60]J. Gersten, in *Topics in Fluorescence Spectroscopy, Vol. 8: Radiative Decay Engineering* (Springer Science + Business Media, New York, 2005).
[61]S. D'Agostino, P. P. Pompa, R. Chiuri, R. J. Phaneuf, D. G. Britti, R. Rinaldi, R. Cingolani, and F. Della Sala, Opt. Lett. **34**, 2381 (2009).
[62]K. J. Vahala, Nature (London) **424**, 839 (2003).
[63]P. Goy, J. M. Raimond, M. Gross, and S. Haroche, Phys. Rev. Lett. **50**, 1903 (1983).
[64]G. Gabrielse and H. Dehmelt, Phys. Rev. Lett. **55**, 67 (1985).
[65]M. Bayer, F. Weidner, A. Larionov, A. McDonald, A. Forchel, and T. L. Reinecke, Phys. Rev. Lett. **86**, 3168 (2001).
[66]E. M. Purcell, Phys. Rev. **69**, 681 (1946).
[67]K. H. Drexhage, Prog. Opt. **12**, 163 (1974).
[68]D. Kleppner, Phys. Rev. Lett. **47**, 233 (1981).
[69]P. Lodahl, A. F. van Driel, I. S. Nikolaev, A. Irman, K. Overgaag, D. Vanmaekelbergh, and W. L. Vos, Nature (London) **430**, 654 (2004).
[70]R. X. Bian, R. C. Dunn, X. S. Xie, and P. T. Leung, Phys. Rev. Lett. **75**, 4772 (1995).
[71]B. C. Buchler, T. Kalkbrenner, C. Hettich, and V. Sandoghdar, Phys. Rev. Lett. **95**, 063003 (2005).
[72]J. D. Jackson, *Classical Electrodynamics*, 3rd ed. (John Wiley and Sons, Berkeley, CA, 1999).
[73]M. A. Yurkin and A. G. Hoekstra, J. Quant. Spectrosc. Radiat. Transfer **112**, 2234 (2011).
[74]A. Moroz, Ann. Phys. (NY) **315**, 352 (2005).
[75]F. De Angelis, G. Das, P. Candeloro, M. Patrini, M. Galli, A. Bek, M. Lazzarino, I. Maksymov, C. Liberale, L. C. Andreani, and E. Di Fabrizio, Nat. Nanotech. **5**, 67 (2010).
[76]F. De Angelis, F. Gentile, F. Mecarini, G. Das, M. Moretti, P. Candeloro, M. L. Coluccio, G. Cojoc, A. Accardo, C. Liberale, R. P. Zaccaria, G. Perozziello, L. Tirinato, A. Toma, G. Cuda, R. Cingolani, and R. Di Fabrizio, Nat. Photon. **5**, 682 (2011).
[77]R. Marty, G. Baffou, A. Arbouet, C. Girard, and R. Quidant, Opt. Express **18**, 3035 (2010).
[78]M. K. Schmidt, S. Mackowski, and J. Aizpurua, Opt. Lett. **37**, 1017 (2012).
[79]M. Liu, T.-W. Lee, S. K. Gray, P. Guyot-Sionnest, and M. Pelton, Phys. Rev. Lett. **102**, 107401 (2009).
[80]M. Mivelle, T. S. van Zanten, L. Neumann, N. F. van Hulst, and M. F. Garcia-Parajo, Nano Lett. **12**, 5972 (2012).
[81]The disappearance of higher order modes with dipole excitation in Fig. 8(a) is not believed to be due to a selection rule, but rather to a very low excitation intensity due to effect of the tip.
[82]J.-S. Huang, V. Callegari, P. Geisler, C. Brning, J. Kern, J. C. Prangsma, X. Wu, T. Feichtner, J. Ziegler, P. Weinmann, M. Kamp, A. Forchel, P. Biagioni, U. Sennhauser, and B. Hecht, Nat. Commun. **1**, 150 (2010).
[83]H. Fischer and O. J. F. Martin, Opt. Express **16**, 9144 (2008).
[84]P. J. Schuck, D. P. Fromm, A. Sundaramurthy, G. S. Kino, and W. E. Moerner, Phys. Rev. Lett. **94**, 017402 (2005).
[85]D. P. Fromm, A. Sundaramurthy, P. J. Schuck, G. Kino, and W. E. Moerner, Nano Lett. **4**, 957 (2004).
[86]J. N. Farahani, D. W. Pohl, H.-J. Eisler, and B. Hecht, Phys. Rev. Lett. **95**, 017402 (2005).
[87]D. P. Fromm, A. Sundaramurthy, A. Kinkhabwala, P. J. Schuck, G. S. Kino, and W. E. Moerner, J. Chem. Phys. **124**, 061101 (2006).
[88]D.-K. Lim, K.-S. Jeon, H.-M. Kim, J.-M. Nam, and Y. D. Suh, Nat. Mater. **9**, 60 (2010).
[89]S. Kim, J. Jin, Y. J. Kim, I. Y. Park, Y. Kim, and S. W. Kim, Nature (London) **453**, 757 (2008).
[90]F. Alpeggiani, S. D'Agostino, and L. C. Andreani, Phys. Rev. B **86**, 035421 (2012).
[91]R. D. Artuso and G. W. Bryant, Nano Lett. **8**, 2106 (2008).